ACS OMEGA

http://pubs.acs.org/journal/acsodf

Article

Bioinformatics and Network Pharmacology of the First Crystal Structured Clerodin: Anticancer and Antioxidant Potential against Human Breast Carcinoma Cell

Sourav Pakrashy, Prakash K. Mandal, Juli Nanda Goswami, Surya Kanta Dey, Sujata Maiti Choudhury, Biswajit Bhattacharya, Franziska Emmerling, Fatmah Ali Alasmary, and Malay Dolai*

Cite This: *ACS Omega* 2022, 7, 48572−48582

Read Online

ACCESS | Metrics & More | Article Recommendations | Supporting Information

ABSTRACT: Clerodin was isolated from the medicinal plant *Clerodendrum infortunatum*, and CSD search showed the first crystal structure of clerodin by a single-crystal X-ray diffraction study. We checked its binding potential with target proteins by docking and conducted network pharmacology analysis, ADMET analysis, in silico pathway analysis, normal mode analysis (NMA), and cytotoxic activity studies to evaluate clerodin as a potential anticancer agent. The cell viability studies of clerodin on the human breast carcinoma cell line (MCF-7) showed toxicity on MCF-7 cells but no toxicity toward normal human lymphocyte cells (HLCs). The anticancer mechanism of clerodin was validated by its enhanced capacity to produce intracellular reactive oxygen species (ROS) and to lower the reduced glutathione content in MCF-7 cells.

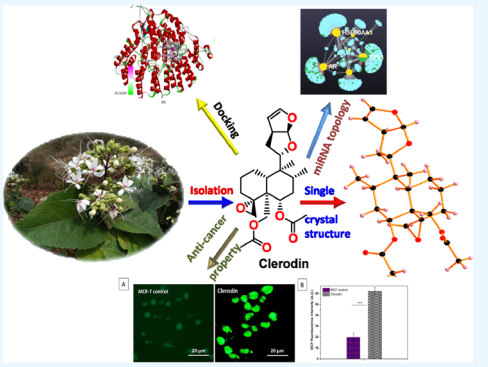

INTRODUCTION

In the last few decades, natural products have been recognized as agents for treating human diseases across the world. Sources of natural products are different, which include plants, vertebrates, invertebrates, microorganisms, and marine organisms.[1] Diversity in natural chemical sources serves as an important cenote of potential bioactive phytocompounds in the development of new leads by providing novel synthons for new drugs, as well as paths for structural architecture to produce highly potent, safe, and cheap drugs. Twenty-five percent of the total drugs are the contribution from medicinal plant-derived natural products,[2] whereas over 60% of all clinically used drugs are inspired by natural products. To name a few, the structural design of metformin used in the treatment of diabetes is inspired by Galegine, a phytoconstituent of *Galega officinalis* L.,[3] and the phytoconstituent Papaverine isolated from *Papaver somniferum*, paving the way for the development of the semisynthetic drug verapamil, which acts as an antihypertensive.[4]

Worldwide, one of the leading causes of death is cancer. The disease is characterized by abnormal burgeoning of cells. Mainly, there are two factors that induce cancer: first, external factors, like alcohol consumption, tobacco consumption, hazardous chemicals, infectious micro-organisms, and radiation; and second, internal factors, which are mutations of a genetic order, mutations that occur from metabolism, up- or down-regulations of some hormones, and critical immune conditions. These factors develop cancer either individually or when performed together synergistically.

In the modern era, the drug discovery and development of plant-based drug discovery has contributed greatly and is still going on to the development and discovery of anticancer leads and drugs in in vitro, in vivo, and clinical trials, as for example, anticancer activity is shown by the extract of *Camptotheca acuminata,* which inspired chemists to isolate its phytoconstituents to check for their anticancer activity individually and sometimes in group, and thus, an anticancer drug in the name of camptothecin was discovered.[5] The uncontrolled growth and spread of cells are commonly referred to as cancer. Therefore, molecules that can inhibit the growth of cells can stop cancer.

One of the widely used medicinal plants is *Clerodendrum infortunatum* because of a major active component, clerodin. It is a diterpenoid, and its anticancer activity will be evaluated through bioassays and bioinformatics. Prior studies have shown that the powder or paste of *C. infortunatum* leaf extracts is reported to be used for the treatment of asthma, pyreticosis, cataract, malaria, and diseases of blood, skin, and lung and showed anti-feedant, cytotoxic, antioxidant, and anti-inflammatory properties. Thus, this plant-derived natural product, clerodin, plays a vital role against some specific disease targets.

Received: November 7, 2022
Accepted: December 1, 2022
Published: December 12, 2022

https://doi.org/10.1021/acsomega.2c07173
ACS Omega 2022, 7, 48572−48582

Scheme 1. Isolation of Clerodin from the Leaves of *C. infortunatum*[a]

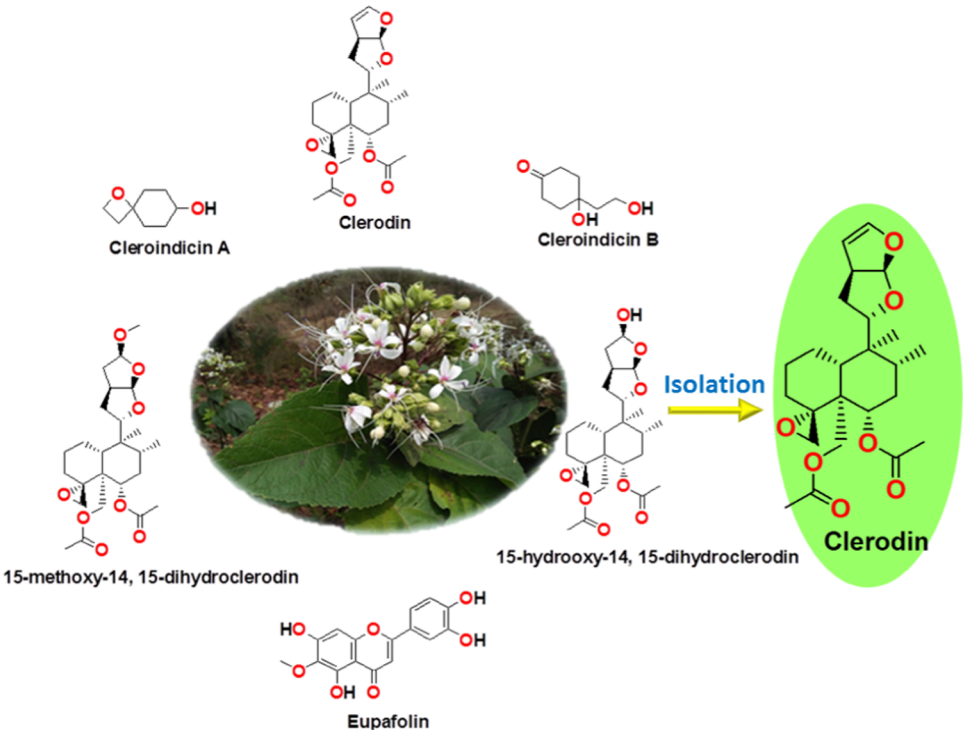

[a]Photograph Courtesy: S. Pakrashy.

For this reason, we have selected the medicinal plant *C. infortunatum* from the genus *Clerodendrum,* which belongs to the family verbenaceae, and isolated a major active component, clerodin, from it.

In this article, we have reported the isolation of clerodin and obtained its first crystal structure. Again, we have performed bioinformatics, network pharmacology studies on Clerodin. Clerodin exhibited anticancer and antioxidant potential against human breast carcinoma cell (MCF-7).

EXPERIMENTAL METHODS AND MATERIALS

Materials. Histopaque 1077, tetrazolium salt 3-(4, 5-dimethylthiazol-2-yl)-2S-diphenyltetrazolium bromide (MTT), penicillin and streptomycin, 2′,7′-dichlorodihydro fluorescein diacetate (H2DCFDA), sulfosalicylic acid, Ellman's reagent (DTNB), and 2-vinyl pyridine were purchased from Sigma-Aldrich Co, LLC. Fetal bovine serum (FBS) and Dulbecco's modified Eagle's medium (DMEM) were purchased from GIBCO.

Isolation of Clerodin. The leaves of *C. infortunatum* (50 g), commonly known as "Bhant" in Hindi and "Ghentu" in Bengali in India, are the only part that people consume; the plant grows throughout the plains of India and is found mostly in West Bengal. For this study, we collected it from local vendors in West Bengal, India. After a while, the leaves were dried in open air and ground with a mortar and pestle. Then, the paste was extracted with 1% ethylacetate in *n*-hexane in a Soxhlet apparatus for 72 h. Using a rotary evaporator, the total extract was then concentrated and kept at room temperature for some time. Then, it was weighed and found to have 2.9 g of yellowish semisolid clay. This clay was then dissolved in chloroform, chromatographed using a silica gel column, and eluted with (1:50) ethylacetate in *n*-hexane.

The fraction obtained with (1:50) ethylacetate in *n*-hexane afforded a green solid, which, after washing with n-hexane, afforded 29 mg of pure clerodin, as green crystals. Then, the structure was confirmed using ^{1}H NMR and X-ray crystallography. Thus, the amount of clerodin (Scheme 1) present in leaves of *C. infortunatum* was found to be 0.058%.

Crystallographic Measurements. The data collection for clerodin was made using a Bruker SMART APEX CCD area detector equipped with a graphite monochromated Mo Kα radiation (λ = 0.71073 Å) source in φ and ω scan modes. Cell parameter refinement and data reduction were carried out using Bruker SMART[20] and Bruker SAINT software for the compound. The structure was solved by conventional direct methods and refined by full-matrix least-square methods using F^2 data. SHELXS-97 and SHELXL-97 programs[21] were used for structure solution and refinement, respectively. Hydrogen atoms on oxygen atoms were found from a Fourier difference map and were allowed to refine while all other hydrogen atoms were placed in calculated positions. Selected crystallographic parameters of clerodin are given in Table 1.

Data Collection. Here, the study was conducted by choosing the compound clerodin, which is an active ingredient of *C. infortunatum* leaves. For execution of network pharmacology and molecular docking with potential cancer protein targets, the genes and their respective proteins were collected from the NCBI gene bank and the Uniprot database. The protein targets were obtained from the RSCB PDB website and considered for the molecular docking study of clerodin.

Molecular Docking. The in silico docking of the compounds, via protein-ligand binding energy (ΔG) analysis, was performed using Auto Dock Vina[6] as an extension in UCSF Chimera.

The protein cyclin-dependent kinase 2,2,5 diaryl isoxazole Hsp 90 Chaperone inhibitor, phosphoinositide 3-kinase,

https://doi.org/10.1021/acsomega.2c07173
ACS Omega 2022, 7, 48572−48582

Table 1. Crystal Data and Details of Structure Determination

crystal data (CCDC-2210102)	
formula	$C_{24}H_{34}O_7$
formula weight	434.51
crystal system	monoclinic
space group	$P2_1$ (No. 4)
a, b, c [Å]	14.8028(12), 9.8415(6), 15.7498(12)
α, β, γ [°]	90, 92.647(3), 90
V [Å^3]	2292.0(3)
Z	4
D(calc) [g/cm^3]	1.259
μ(Mo Kα) [/mm]	0.092
F(000)	936
data collection	
temperature (K)	150
radiation [Å]	0.71073
θ min−max [°]	2.6, 28.3
data set	−19: 19; −13: 13; −21: 20
tot., uniq. data, R(int)	38309, 11267, 0.052
observed data [$I > 2.0\ \sigma(I)$]	9550
refinement	
N_{ref}, N_{par}	11267, 568
R, wR2, S	0.0781, 0.2488, 1.05

farnesyltransferase, androgen receptor, human p53 core domain mutant N235K, and β-hexosaminidase B were retrieved from the RCSB Protein DataBank (PDB) (http://www.rcsb.org/pdb), PDB-ID 2R3J, 2VCJ, 4FLH, 1JCQ, 2PIT, 4LO9, and 1NOW in the PDB format; all of the proteins have good ligand structure goodness of fit to experimental data. As per the docking protocol, removal of all water and solvent molecules, cocrystallized residues (if any), and mirror chain (if any) was ensured using UCSF Chimera software. Next is the protein structure preparation, and it is also done in Chimera. The protein structures were prepared by assigning hydrogen atoms, charges, and energy minimization using the Dock Prep tool. The charges were assigned as per the AM1-BCC method, which quickly and efficiently generates high-quality atomic charges for protein, and the charges were computed using the ANTECHAMBER algorithm.[7] Energy minimization was performed using the swiss pdb (SPDBV)[8] viewer. The target proteins after minimization of energy were then saved in the PDB format for future docking purposes.

Clerodin, used for the in silico interaction assays, is the medicinal plant's secondary metabolites, which is present in PubChem, PubChem ID−442014, retrieved from there in the SMILE format, copied and pasted in ChemDraw and cleaned up, after which it was copied to Chem3D pro, where its energy minimization was carried using MM2 calculations, after which it was saved in the SDF (3D) format. Now, before performing the molecular docking of the ligand and the protein, the ligands were optimized by addition of hydrogen and addition of charge using the Gasteiger algorithm,[9] and energy minimization was performed using 1000 steepest descent steps with a 0.02 Armstrong step size with an update interval of 10 and then again saved in PDB format in the structure editing wizard of Chimera software, which is driven by the chemoinformatic principle of electronegativity equilibration, and then the files were saved in the PDB format. A grid box that assigns the binding region was chosen in such a way that it would cover the protein's active site for the hydrophobic surface of the concave region of the protein to fit in properly the hydrophobic surface of the ligand giving the best binding score. For visualizing in different formats, we used the software Discovery studio and UCSF Chimera.

Network Pharmacology. It is a vast section that describes the relationship between genes that are responsible for causing diseases and the action of drugs. Here, we will use it to find the connection between the genes (causative agents of cancer). By exploring research journals of PubMed, we found a group of seven genes responsible for different forms of cancer, namely, CDK2,[10] HSP90AA1,[11] PIK3CG,[12] FNTA,[13] AR,[14] TP53,[15] and HEXB.[16] We created an interaction network with these seven genes of interest using STRING-DB, an online tool, and used Cytoscape[17] software to figure out the most connected gene. These genes gave the seven target proteins we considered here for docking.

Enrichment analysis was done to characterize a gene list, and we will use it to find its KEGG pathway. An online tool Enrich R was used to perform this analysis.

To identify micro-RNAs associated with the seven genes, we will use another online tool miRNet; micro-RNAs can regulate gene expression, and these are noncoding RNAs.

ADMET Prediction. In silico ADME analysis was conducted to investigate the physical-chemical properties of the potent hits, such as water solubility, lipophilicity, bioradar (for orally acceptable molecules), drug likeness, and pharmacokinetics using the following website http://www.swissadme.ch. However, the toxicity of these molecules could not be investigated using SwissADME;[18] thus, the pkCSM[19] pharmacokinetics server was used to predict the toxicity properties of the molecules with their SMILE (simplified molecular input line entry specification) profile.

Cutoff parameters set were that the compound should not be a blood−brain barrier (BBB) permeate and should not react with any cytochrome P450 enzyme.

Molecular Dynamic Simulation. Molecular dynamics simulation studies of docked complexes play a crucial part in validating the drug candidate and protein fit binding. Molecular dynamics was carried out with the iMODS[22] server to explain the usual protein motion within the internal coordinates through normal mode analysis (NMA). iMODS is a highly customizable and useful server and shows a number of levels, which are coarse-grained (CG). It predicts the dihedral coordinates of Cα atoms with large calculations of these big docked complexes. Furthermore, the B-factor is also predicted in the iMODS server along with structural deformability and determines the eigenvalue.

Methods for Isolation of Human Lymphocyte Cells (HLCs). In heparin-coated vacutainers, 5 mL of blood sample was collected from healthy young volunteers using the method of Hudson and Hay.[23] Then, 4 mL of blood was taken in a centrifuge tube and the same volume of Histopaque 1077 (Sigma-Aldrich Co. LLC) was added to it. The blood sample was then centrifuged at 2000 rpm for 20 min at room temperature, and the lymphocyte monolayer was collected and transferred to a fresh autoclaved centrifuge tube. The HLC cells were washed 3 times in a phosphate-buffered solution (pH 7.4), resuspended in an RPMI medium supplemented with 10% FBS, and incubated in a CO_2 incubator for 24 h at 37 °C.

Cell Viability Study. MCF-7 cells were obtained from Chittaranjan National Cancer Institute, Kolkata-700 026 West Bengal, India. Cells were cultured in DMEM supplemented with 10% FBS, penicillin (100 U mL^{-1}), and streptomycin (10 mg/mL) in a humidified atmosphere of 5% CO_2 at 37 °C.

https://doi.org/10.1021/acsomega.2c07173
ACS Omega 2022, 7, 48572−48582

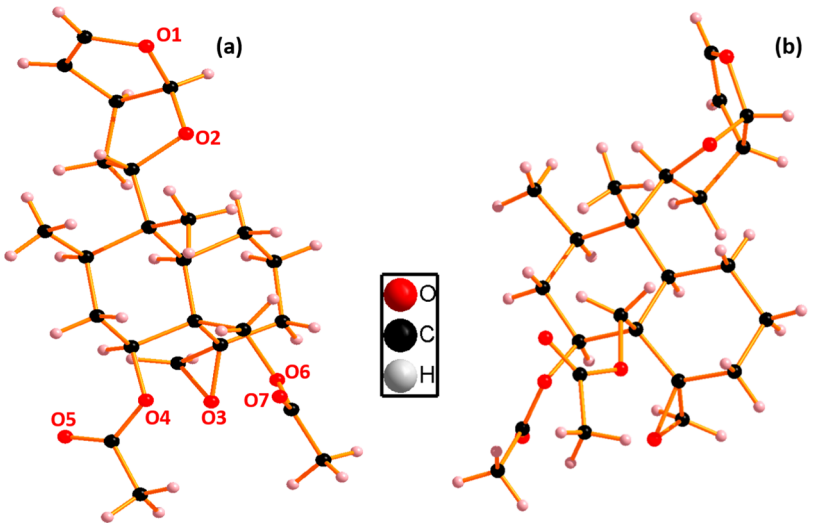

Figure 1. Crystal structure: top view (a) and side view (b) of clerodin. Color code: red, oxygen; black, carbon; off-white, hydrogen.

Cell viability studies of clerodin in human lymphocyte cells (HLCs) and MCF-7 cells were performed by a tetrazolium salt 3-(4, 5-dimethylthiazol-2-yl)-2S-diphenyltetrazolium bromide (MTT) assay.[24] In brief, cells were seeded in 96-well plates at a density of 1×10^6 cells per well in 100 μL of culture medium and incubated with a series of concentrations (0.5, 1, 2, 5, 10, 25, 50, and 100 μg/mL) of clerodin at 37 °C in a CO_2 incubator for 24 h. After 24 h of treatment, the culture medium was removed and cells were washed with PBS (pH 7.4). After adding 10 μL of a stock MTT solution (5 mg/mL) into each well, it was again incubated for 3 h at 37 °C. The formed intracellular formazan crystal (blue-violet) was dissolved with the addition of 0.1% DMSO, and absorption was measured at the wavelength of 540 nm by an ELISA ANALYSER (Bio-Rad, Model 680). The cytotoxicity of clerodin was studied by calculating the value of the inhibitory concentration (IC_{50}), and the cell viability was measured using the following formula. Values are mean (M) ± standard error of mean (SEM) of three independent experiments.

$$\%\ \text{cell viabilty} = (\text{OD of sample})/(\text{OD of control}) \times 100$$

Measurement of Intracellular ROS Generation. Intracellular ROS generation was measured using 2′,7′-dichlorodihydro fluorescein diacetate (H_2DCFDA).[23] MCF-7 cells were cultured for 24 h and treated with clerodin at its IC_{50} dose (30.88 μg/mL) for another 24 h. After that, the DMEM media was discarded and cells were washed with phosphate-buffered saline (PBS, pH 7.4) and then incubated with H_2DCFDA (1 μg/mL) for 30 min at 37 °C followed by washing with PBS three times. Finally, oxidation of DCFH-DA to 2′-7′dichlorofluorescein (DCF) was quantified using a Hitachi F-7000 fluorescence spectrophotometer at 485 nm (excitation) and 520 nm (emission). The image was taken by fluorescence microscopy (LEICA DFC295, Germany).

Estimation of Reduced Glutathione (GSH) and Oxidized Glutathione (GSSG). To estimate reduced glutathione (GSH), 0.2 mL of the test sample was mixed with sulfosalicylic acid (4%) and the mixture was centrifuged at 2000 rpm for 10 min. After that, the supernatant was aspirated and 2 mL of DTNB solution (0.6 mM) was added to it. A yellow-colored complex was formed by the reaction of DTNM and GSH, and this was measured by a spectrophotometer at 412−420 nm.[23,24]

Oxidized glutathione (GSSG) was measured by derivatization of GSH with 2-vinyl pyridine with a slight modification. In brief, 2 mL of 2-vinyl pyridine was mixed with 0.1 mL of the test sample followed by incubation for 1 h at 37 °C. Sulfosalicylic acid (4%) was added to the mixture and centrifuged at 3000 rpm for 10 min. The supernatant was taken, and the amount of GSSG level was measured using the above method. The experiment was performed in triplicate, and the results are expressed as mean ± SEM.[23]

RESULTS AND DISCUSSION

Isolation and Structural Description of Clerodin. The fraction obtained from the leaves of *C. infortunatum*, commonly known as "Ghentu" in Bengali, with (1:50) ethyl acetate in *n*-hexane afforded a green solid, which, after washing with n-hexane, afforded pure clerodin, as green crystals. The structure was confirmed by ^{1}H NMR and single-crystal X-ray crystallography.

The unequivocal single-crystal X-ray structural proof of the asymmetric unit of clerodin with top and side views is shown in Figure 1. The clerodin crystallized in the monoclinic system with the space group $P2_1$. The unit cell is composed of two molecules. The molecule consists of a (5,5) fused furo[2,3-*b*] furan ring moiety (oxygen named O1 and O2) and adopts a half-chair conformation, as evidenced by the crystal structure. Only one bridged-headed epoxide (O3) and two acetates (O4 and O6) as ester functional groups are attached with a fused bicyclic ring, which gives the compound a puckering structure. The crystallographic parameters are given in Table 1.

Docking Studies. The protein ligand binding interactions (Table 2) between the targeted proteins PDB-ID 2R3J, 2VCJ, 4FLH, 1JCQ, 2PIT, 4LO9, and 1NOW and the ligand clerodin, which is the main phytocompound of the leaves of our medicinal plant *C. infortunatum*, were determined using molecular docking. The calculations reveal the highest free energy change for these interaction as $\Delta G = -8.2$ Kcal/mol of clerodin for the protein farnesyltransferase 1JCQ inside a grid box of 15.6 × 129 × −2.51 Å^3 with size 30 × 30 × 30 Å^3 along the *x*-, *y*-, and *z*-axes (Figure 2). The calculations reveal the second highest free energy change for these interactions as $\Delta G = -7.9$ Kcal/mol

https://doi.org/10.1021/acsomega.2c07173
ACS Omega 2022, 7, 48572−48582

Table 2. Results of the Docking of Clerodin and Target Proteins

name of protein targets	PDB ID	docking score (Kcal/mol) Clerodin
(1) cyclin-dependent kinase 2	2R3J no mutation human	−6
(2) Hsp 90 chaperone inhibitor	2VCJ no mutation human	−5.8
(3) phosphoinositide 3-kinase	4FLH no mutation human	−7.9
(4) farnesyltransferase	1JCQ no mutation human	−8.2
(5) androgen receptor	2PIT No mutation human	−6
(6) human p53 core domain mutant N235K	4LO9 yes mutation human	−5.1
(7) β-hexosaminidase B	1NOW no mutation human	−7

clerodin for the protein phosphoinositide 3-kinase 4FLH inside a grid box of 19.1 × 16.05 × 23.12 Å^3 with size 31.1 × 40.5 × 31.61 Å^3 along the *x*-, *y*-, and *z*-axes (Figure 3).

DOCKING RESULTS

ADME PREDICTION RESULTS

The result from SWISS ADME is very satisfactory as clerodin shows no disagreement with any of the drug-likeness property, and it has high gastrointestinal absorption and is soluble in water as well; moreover, it has a good bioradar (Figure 4), which makes it orally admissible to people. Clerodin does not inhibit any of the cytochrome P50 enzymes and is also not a PGP substrate.

It has a good log *P* value of 2.88, which is essential for showing drug-like properties (Table 3). The total polar surface area (TPSA) of clerodin is also good.

From the pKCSM server, we predicted the toxicity of clerodin, and the result was very promising: clerodin offers no hepatotoxicity, no ADMES toxicity, and a small toxicity of 1.99.

NETWORK PHARMACOLOGY

Network pharmacology revealed that only five out of seven genes are connected (Figure 5) with each other, namely, CDK2, HSP90AA1, PIK3CG, AR, and TP53, resulting from STRING-DB, the online web portal, and the remaining two are not connected with these five and each other and may be considered individual participants.

Using Cytoscape, we found that among the five connected genes, TP53 has the maximum connections, while PIK3CG has only one connection, that too with TP53.

The Kaplan−Meier plot revealed that the CDK2 gene showed median survival, the HSP90AA1 gene showed median survival, the PIK3CG gene showed upper quartile survival, the FNTA gene showed median survival, the AR gene showed upper

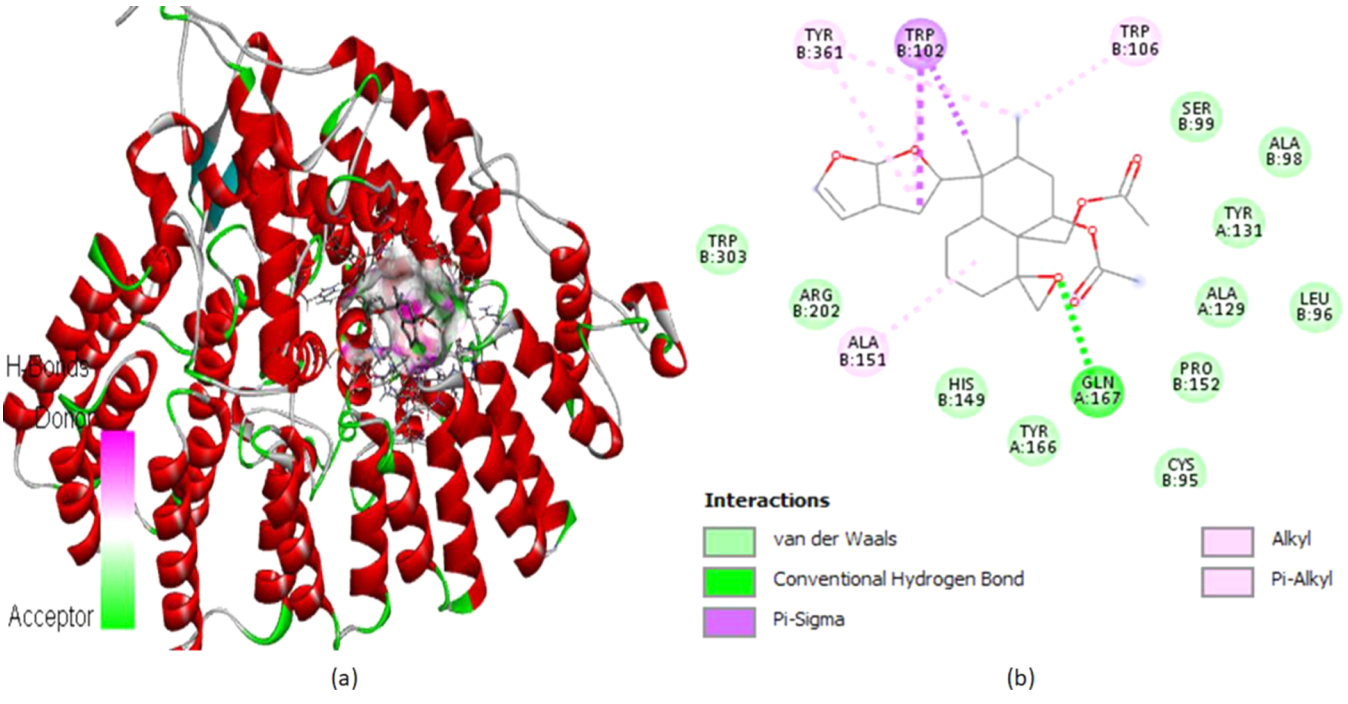

Figure 2. Docking poses of clerodin with 1JCQ.

https://doi.org/10.1021/acsomega.2c07173
ACS Omega 2022, 7, 48572−48582

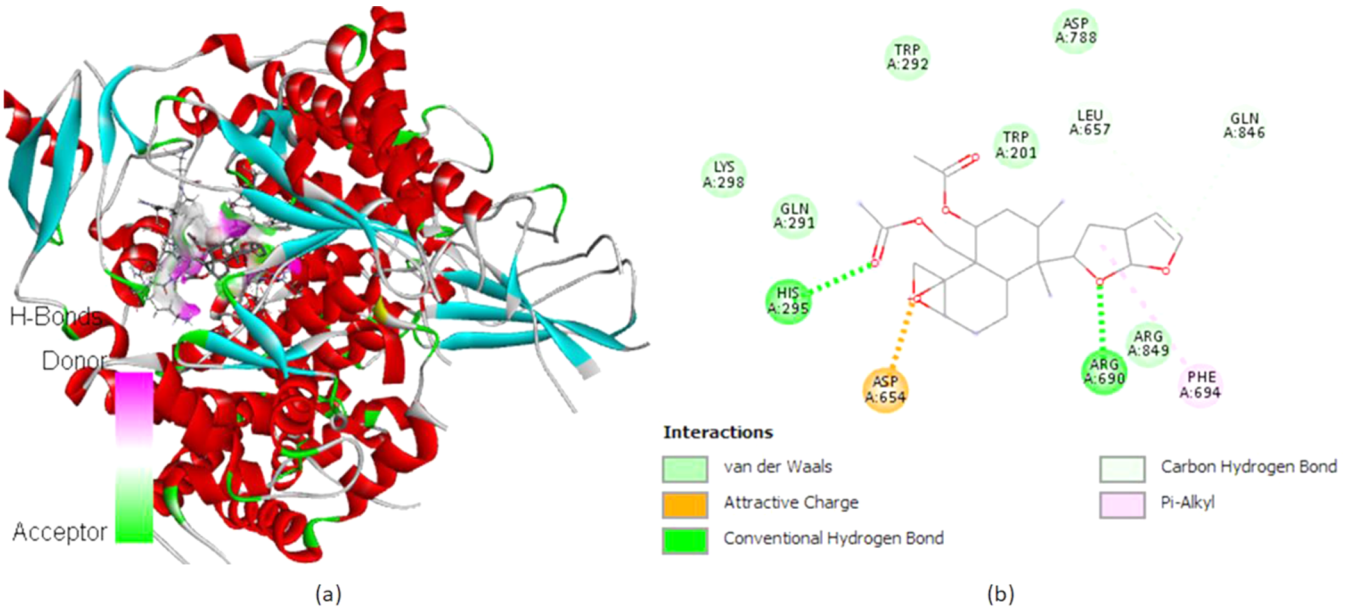

Figure 3. Docking poses of clerodin with 4FLH.

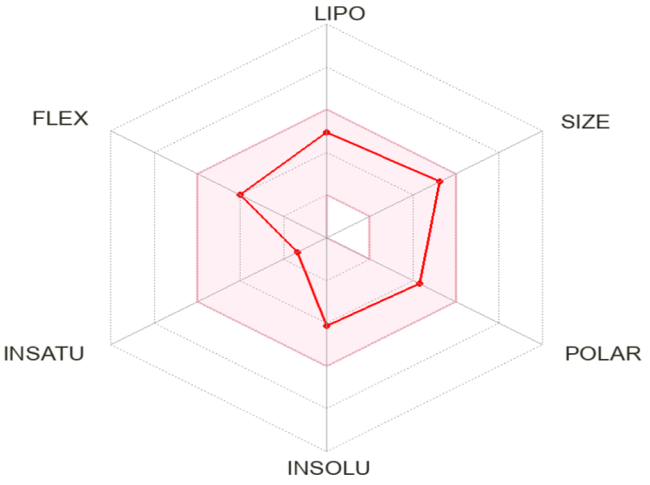

Figure 4. Bioradar of clerodin for oral bioavailability.

quartile survival, the TP53 gene showed median survival, and the HEXB gene showed median survival. Other information that is retrieved from this server is low expression cohort (LEC) in months, high expression cohort (HEC) in months, log rank P, and hazard ratio (Table 4). The plots are shown in Figure 7.

KEGG pathway analysis from the Enrich R web server enlightened us by providing 10 significant pathways related to these seven genes. These pathways are prostate cancer, PI3K-Akt signalling pathway, pathways in cancer, p53 signalling pathway, small-cell lung cancer, progesterone-mediated oocyte maturation, cell cycle, oocyte meiosis, measles, fluid shear stress, and atherosclerosis.

Micro-RNA analysis (Figure 6) resulted in a number of micro-RNAs, which are named as miR followed by the respective number and are denoted in skyish blue, the transcription factors are in green, and the genes are in yellow. TP53 is the most connected gene and is also a transcription factor. Some other transcription factors are AATF, DNMT1, etc. (Figure 7).

Table 3. Physicochemical and Drug-Like Properties of Clerodin

physicochemical properties		pharmacokinetics	
formula	$C_{24}H_{34}O_7$	GI absorption	high
molecular weight	434.52 g/mol	BBB permeant	no
num. of heavy atoms	31	P-gp substrate	no
num. of arom. heavy atoms	0	CYP1A2 inhibitor	no
fraction Csp3	0.83	CYP2C19 inhibitor	no
num. of rotatable bonds	6	CYP2C9 inhibitor	no
num. of H-bond acceptors	7	CYP2D6 inhibitor	no
num. of H-bond donors	0	CYP3A4 inhibitor	no
molar refractivity	111.78	log K_p (skin permeation)	−6.72 cm/s
TPSA	83.59 Å^2		
lipophilicity		drug-likeness	
log $P_{o/w}$ (iLOGP)	2.88	Lipinski	yes; 0 violation
log $P_{o/w}$ (XLOGP3)	3.14	Ghose	yes
log $P_{o/w}$ (WLOGP)	3.36	Veber	yes
log $P_{o/w}$ (MLOGP)	2.45	Egan	yes
log $P_{o/w}$ (SILICOS-IT)	3.21	Muegge	yes
consensus log $P_{o/w}$	3.01	bioavailability score	0.55
		Lipinski	yes; 0 violation
		Ghose	yes
		Veber	yes
		Egan	yes

MOLECULAR DYNAMICS SIMULATION

Molecular dynamics simulation study of docked complexes plays a crucial part in validating the secondary metabolites and protein fit binding, which can be shown as a comparison in the normal mode of the prepared protein analysis dynamics. In this case, a dynamics study of the essential protein docked complexes was applied to the selected number of normal modes of the prepared

https://doi.org/10.1021/acsomega.2c07173
ACS Omega 2022, 7, 48572−48582

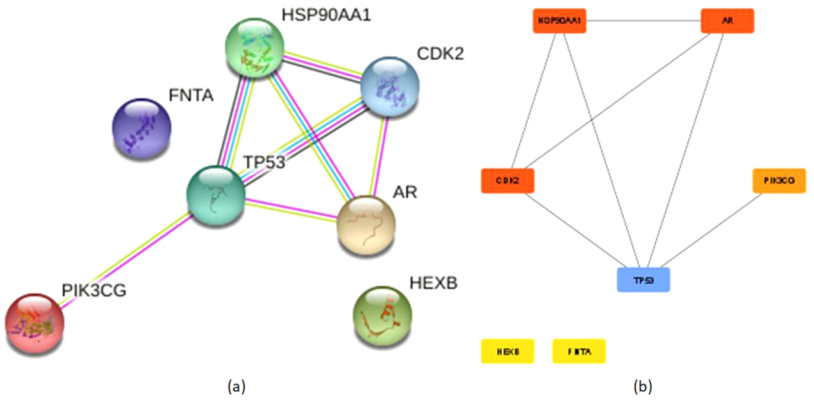

Figure 5. (a) Interactions from STRING-DB. (b) Interactions from cytoscape.

Table 4. Kaplan−Meier Plot Results

gene symbol	LEC (months)	HEC (months)	Log rank P	hazard ratio
CDK2	216.66	228.25	0.2	1.07
HSP90AA1	216.66	185.16	1.2×10^{-11}	1.42
PIK3CG	35	46.49	4.4×10^{-5}	0.73
FNTA	216.66	184.04	1.5×10^{-5}	1.25
AR	44	55.06	0.0034	0.86
TP53	185.16	216.66	0.023	0.89
HEXB	216.66	228.85	0.18	1.07

protein to determine its mobility, rigidness, and stability through the iMODS server. In this case, the study comprises the binding dynamics (Figure 8) of the top two docked complexes of the compound clerodin with the targeted proteins 1JCQ and 4FLH.

B-factor values showed the amplitude relative to the displacement of atoms around the state of equilibrium and with the help of NMA, which can be considered equivalent of or close to the RMS; thus, we will be able to understand the range of inhibition of action when will be subjected to real experiments in vitro (Figure 8).

Deformability gives an idea about a molecule's flexibility to deform from its original orientation. Hinges at specific sites represent the binding of the molecule at the respective site (Figure 8).

CELL VIABILITY STUDY

Cell viability studies of HLCs and MCF-7 cells were studied by an MTT assay.[25−28] The result showed that clerodin significantly inhibited MCF-7 cell viability in a concentration-dependent manner as compared to the MCF-7 control group (Figure 9A). Clerodin was found to be a potent cytotoxic agent against MCF-7 cells, and the IC_{50} value was found to be 30.88 ± 2.06 μg/mL. On the other hand, clerodin exhibited 51 and 28% cell viabilities at concentrations of 25 and 100 μg/mL, respectively (Figure 9B). It is assumed that clerodin can be used safely up to 50 μg/mL.

Intracellular ROS Generation Study. Oxidative stress is a state in which excessive reactive oxygen species (ROS) were produced due to the failure of the intracellular antioxidant defence mechanism. This caused severe oxidative damage to DNA, lipids, and sugars.[29] Glutathione (GSH) played a significant role in controlling ROS generation and thereby helped maintain redox homeostasis. An elevated level of GSH was observed in cancer cells, which may help detoxify xenobiotics.[30] This is the reason why GSH has gained the attention of researchers for cancer therapy.

Results showed that the fluorescence intensity of DCF was significantly ($P < 0.001$) increased after the treatment with clerodin compared to the MCF-7 control group (Figure 10A). This may be due to the conversion of nonfluorescent H_2DCFDA to the highly fluorescent 2′,7′-dichlorofluorescein (DCF) by oxidation reaction in the presence of excessive free radicals. The

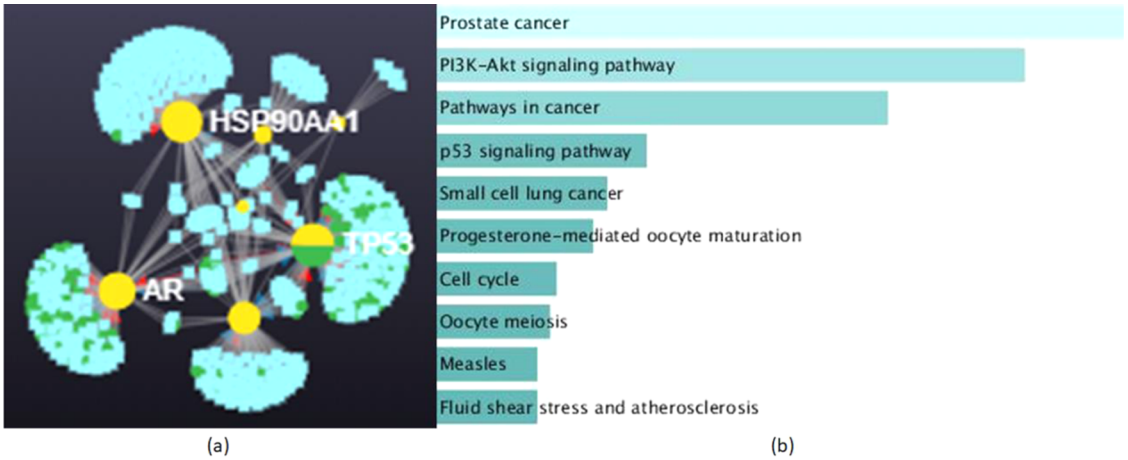

Figure 6. (a) miRNA topology from miRNet. (b) KEGG_2021 bar graph (human).

https://doi.org/10.1021/acsomega.2c07173
ACS Omega 2022, 7, 48572−48582

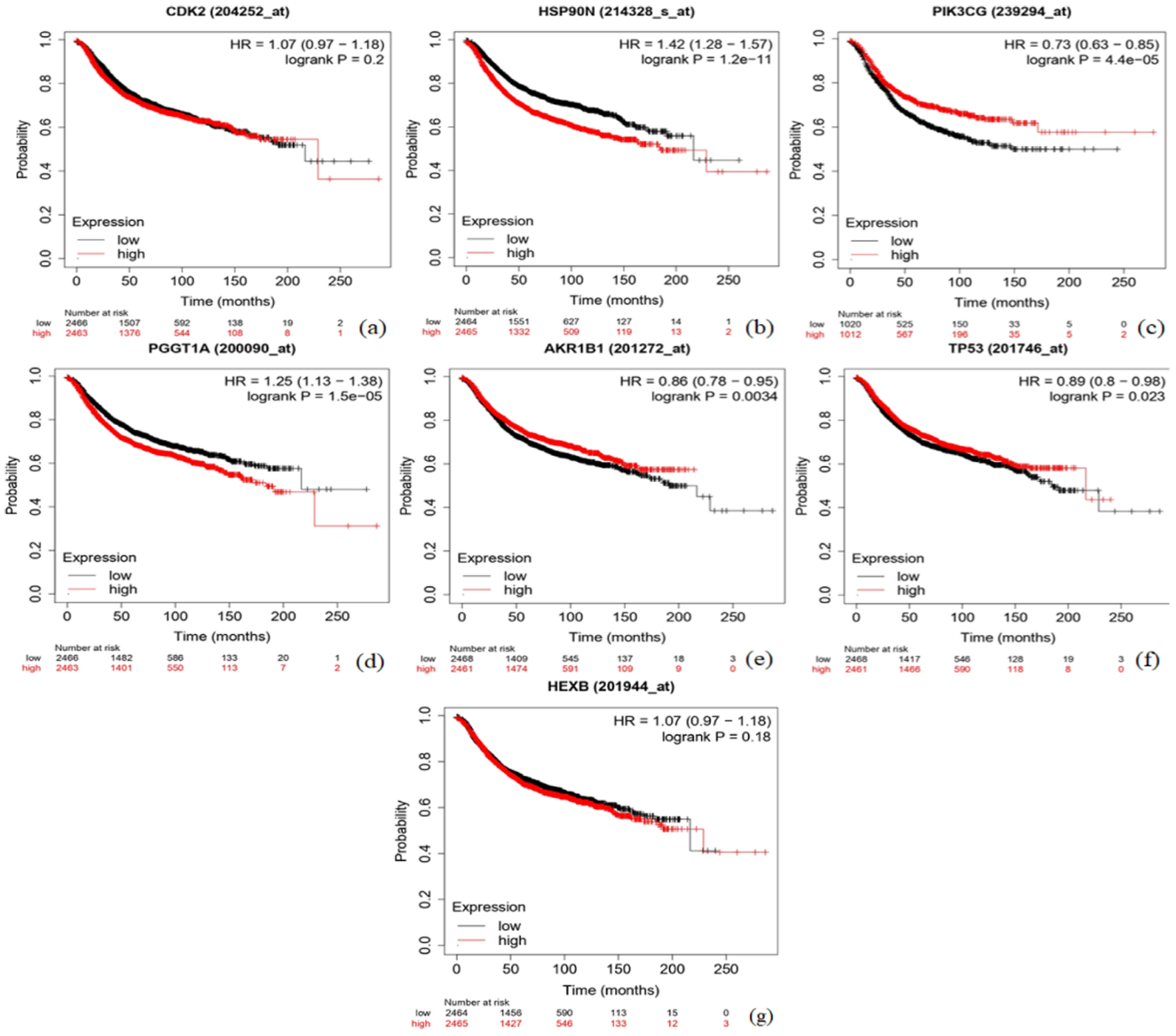

Figure 7. Kaplan−Meier plots of (a) CDK2, (b) HSP90AA1, (c) PIK3CG, (d) FNTA, (e) AR, (f) TP53, and (g) HEXB genes from the server.

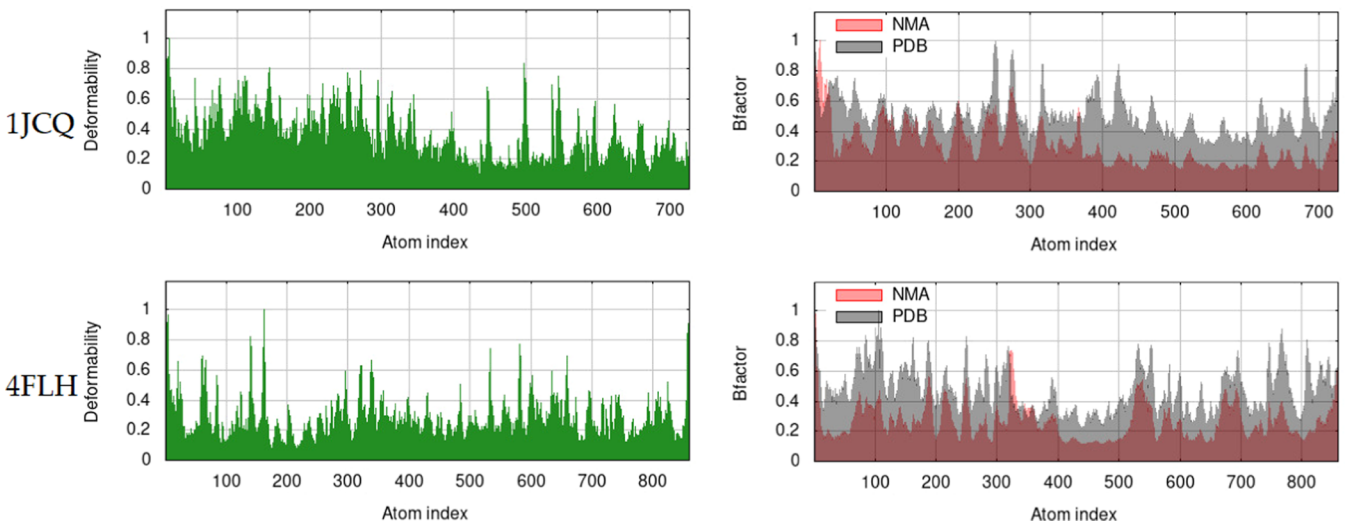

Figure 8. Deformability and B-factor of clerodin-bonded 1JCQ and 4FLH.

https://doi.org/10.1021/acsomega.2c07173
ACS Omega 2022, 7, 48572−48582

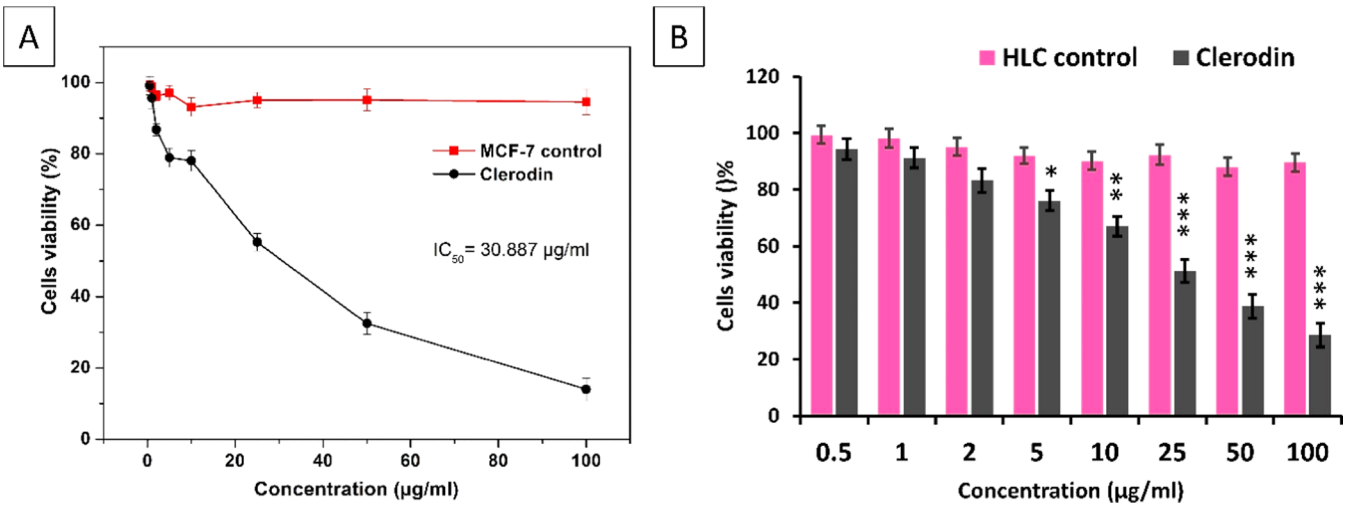

Figure 9. Cytotoxicity study of clerodin on MCF-7 cells and human lymphocyte cells (HLCs) by the MTT assay. Cells were treated with different concentrations (0.5−100 μg/mL) of clerodin for 24 h in a CO_2 incubator. The IC_{50} value was found to be 30.88 ± 2.06 μg/mL for MCF-7 cells (A). Clerodin showed a concentration-dependent cell viability assay in HLCs cells (B). Values are expressed as the mean ± SEM. (*p < 0.5; **p < 0.01; ***p < 0.001; n = 3).

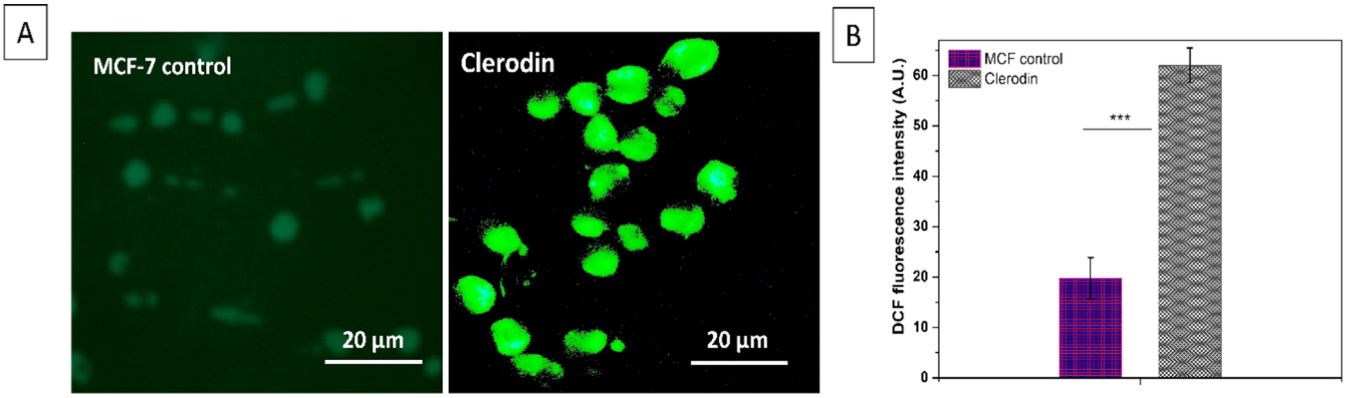

Figure 10. Fluorescence microscopic image of reactive oxygen species (ROS) generation in MCF-7 cells using H_2DCFDA stain after the treatment with clerodin. The scale bar is 20 μm (A). Measurement of the dichlorofluorescein (DCF) fluorescence intensity induced by clerodin in MCF-7 cells (B). Values are expressed as the means ± SEM of three experiments; ***p < 0.001, compared with the control group.

fluorescence microscope image shows a bright-green color, which indicates the generation of intracellular ROS (Figure 10B).

REDUCED GLUTATHIONE (GSH) AND OXIDIZED GLUTATHIONE (GSSG)

Conversion of GSH to glutathione disulfide (GSSG) by oxidation occurred in different pathological conditions, leading to oxidative stress.[31] The present study revealed that the cellular GSH level significantly (p < 0.01) decreased after the treatment with clerodin compared to clerodin untreated cells (Figure 11). The study clearly indicates that the effective conversion of GSH to GSSG was induced by clerodin, which may be due to the excessive ROS generation in MCF-7 cells.

The redox homeostasis is disrupted by the loss of GSH and leads to ROS accumulation, which triggers cell dysfunction and death. In cancer cells, high levels of oxidative stress cause them to be more sensitive to GSH deficiency, which is a fatal weakness, and can be utilized in cancer therapy.[30]

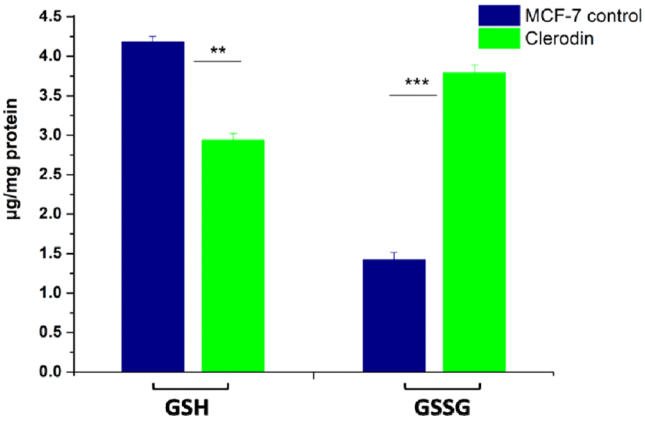

Figure 11. Effect of clerodin on reduced glutathione (GSH) and oxidized glutathione (GSSG) in MCF-7 cells. Values are expressed as the means ± SEM of three experiments; **p < 0.01; ***p < 0.001, compared with the control group.

https://doi.org/10.1021/acsomega.2c07173
ACS Omega 2022, 7, 48572−48582

CONCLUSIONS

The compound clerodin, which is an active ingredient of *C. infortunatum*, present in its leaves in appreciable amounts, serves as a good drug candidate against cancer as evidenced by docking studies along with other scientific approaches. This medicinal plant has various ethno-pharmacological and ethno-botanical importances, which lead us to isolate the major active principles clerodin, which may cure breast cancer by binding with farnesyl transferase and phosphoinositide 3-kinase, two proteins that are required for transforming cells to oncogenic mutants. Clerodin was isolated and first structurally characterized by single-crystal X-ray diffraction and ^{1}H NMR. Then, it has a good chemical structure backbone to exhibit a biological role that significantly inhibited human breast carcinoma cells (MCF-7) by cell viability and decreased cellular GSH level, clerodin has an IC_{50} value of 30.88 ± 2.06 μg/mL. Thus, it can cause death of cancerous cells without affecting normal cells. The plant species is nontoxic and highly valued for its characteristic medicinal importance in the indigenous system of medicine. Toxicity predictions further revealed the nontoxic nature of clerodin. Thus, clerodin could be a good drug candidate for human breast cancer in the near future.

ASSOCIATED CONTENT

Supporting Information

The Supporting Information is available free of charge at https://pubs.acs.org/doi/10.1021/acsomega.2c07173.

ADMET properties of clerodin from the pK-CSM server; receptor interaction at the binding site of other targeted proteins; and ^{1}H NMR spectra of clerodin (PDF)

Accession Codes

The single-crystal X-ray data deposition code is CCDC no.-2210102.

AUTHOR INFORMATION

Corresponding Author

Malay Dolai − *Department of Chemistry, Prabhat Kumar College, Contai 721404 West Bengal, India;* orcid.org/0000-0001-7697-3376; Email: dolaimalay@yahoo.in

Authors

Sourav Pakrashy − *Department of Chemistry, Prabhat Kumar College, Contai 721404 West Bengal, India;* orcid.org/0000-0002-7620-5382

Prakash K. Mandal − *Department of Chemistry, University of Calcutta, Kolkata 700003 West Bengal, India*

Juli Nanda Goswami − *Department of Chemistry, Prabhat Kumar College, Contai 721404 West Bengal, India*

Surya Kanta Dey − *Biochemistry, Molecular Endocrinology, and Reproductive Physiology Laboratory, Department of Human Physiology, Vidyasagar University, Midnapore 721102 West Bengal, India*

Sujata Maiti Choudhury − *Biochemistry, Molecular Endocrinology, and Reproductive Physiology Laboratory, Department of Human Physiology, Vidyasagar University, Midnapore 721102 West Bengal, India*

Biswajit Bhattacharya − *BAM Federal Institute for Materials Research and Testing, 12489 Berlin, Germany;* orcid.org/0000-0003-4138-1287

Franziska Emmerling − *BAM Federal Institute for Materials Research and Testing, 12489 Berlin, Germany;* orcid.org/0000-0001-8528-0301

Fatmah Ali Alasmary − *Department of Chemistry, College of Science, King Saud University, Riyadh 11451, Saudi Arabia*

Complete contact information is available at: https://pubs.acs.org/10.1021/acsomega.2c07173

Notes

The authors declare no competing financial interest.

ACKNOWLEDGMENTS

M.D gratefully acknowledges the I-STEM/catalytic grant/acad-08/2021-2022 for the research support. The authors acknowledge Dr. Ashok Maiti, MD Pathologist, Medipath Diagnostic and Consultation Centre, Midnapore, Paschim Medinipur, West Bengal, India, for the collection of healthy human blood samples for the accomplishment of the MTT assay of human lymphocyte cells. F. A. Alasmary is thankful to the researcher supporting project (RSP-2021/259), King Saud University, Riyadh, Saudi Arabia.

REFERENCES

(1) Newman, D. J.; Cragg, G. M.; Snader, K. M. The influence of natural products upon drug discovery. *Nat. Prod. Rep.* **2000**, *17*, 215−234.

(2) Matatiken, D.; Hoareau, L.; Kante, M.; Mougal, J.; Rene, P.; Rosalie, M.; Spiro, R.; Vidot, F. Conservation and management of medicinal plants: Experiences from seychelles. *Asian Biotechnol. Dev. Rev.* **2011**, *13*, 61−75.

(3) Cragg, G. M.; Newman, D. J. Natural products: A continuing source of novel drug leads. *Biochim. Biophys. Acta, Gen. Subj.* **2013**, *1830*, 3670−3695.

(4) Fabricant, D. S.; Farnsworth, N. R. The value of plants used in traditional medicine for drug discovery. *Environ. Health Perspect.* **2001**, *109*, 69−75.

(5) Kaur, R.; Sharma, A.; Kumar, R.; Kharb, R. Rising Trends towards Herbal Contraceptives. *J. Nat. Prod. Plant Resour.* **2011**, *1*, 5−12.

(6) Allouche, A. Software News and Updates Gabedit - A Graphical User Interface for Computational Chemistry Softwares. *J. Comput. Chem.* **2012**, *32*, 174−182.

(7) Pakrashy, S.; Mandal, P. K.; Dey, S. K.; Choudhury, S. M.; Alasmary, F. A.; Almalki, A. S.; Islam, M. A.; Dolai, M. Design of a Structurally Novel Multipotent Drug Candidate by the Scaffold Architecture Technique for ACE-II, NSP15, and MproProtein Inhibition: Identification and Isolation of a Natural Product to Prevent the Severity of Future Variants of Covid 19 and a a Colorectal Anticancer Drug. *ACS Omega* **2022**, *7*, 33408−33422.

(8) Wang, J.; Wang, W.; Kollman, P.; Case, D. Antechamber, An Accessory Software Package For Molecular Mechanical Calculations. *J. Am. Chem. Soc.* **2001**, *222*, U403.

(9) Guex, N.; Peitsch, M. C. SWISS-MODEL and the Swiss-PdbViewer: An environment for comparative protein modeling. *Electrophoresis* **1997**, *18*, 2714−2723.

(10) Gasteiger, J.; Jochum, C. An Algorithm for the Perception of Synthetically Important Rings. *J. Chem. Inf. Comput. Sci.* **1979**, *19*, 43−48.

(11) Tadesse, S.; Anshabo, A. T.; Portman, N.; Lim, E.; Tilley, W.; Caldon, C. E.; Wang, S. Targeting CDK2 in cancer: challenges and opportunities for therapy. *Drug Discovery Today* **2020**, *25*, 406−413.

(12) Xiao, X.; Wang, W.; Li, Y.; Yang, D.; Li, X.; Shen, C.; Liu, Y.; Ke, X.; Guo, S.; Guo, Z. HSP90AA1-mediated autophagy promotes drug resistance in osteosarcoma. *J. Exp. Clin. Cancer Res.* **2018**, *37*, No. 201.

(13) Semba, S.; Itoh, N.; Ito, M.; Youssef, E. M.; Harada, M.; Moriya, T.; Kimura, W.; Yamakawa, M. Down-regulation of PIK3CG, a catalytic subunit of phosphatidylinositol 3-OH kinase, by CpG hypermethylation in human colorectal carcinoma. *Clin. Cancer Res.* **2002**, *8*, 3824−3831.

(14) Chin, K.; DeVries, S.; Fridlyand, J.; Spellman, P. T.; Roydasgupta, R.; Kuo, W. L.; Lapuk, A.; Neve, R. M.; Qian, Z.; Ryder, T.; Chen, F.; Feiler, H.; Tokuyasu, T.; Kingsley, C.; Dairkee, S.; Meng, Z.; Chew, K.; Pinkel, D.; Jain, A.; Ljung, B. M.; Esserman, L.; Albertson, D. G.; Waldman, F. M.; Gray, J. W. Genomic and transcriptional aberrations linked to breast cancer pathophysiologies. *Cancer Cell* **2006**, *10*, 529−541.
(15) Balk, S. P.; Knudsen, K. E. AR, the cell cycle, and prostate cancer. *Nucl. Recept. Signaling* **2008**, *6*, No. nrs.06001.
(16) Petitjean, A.; Achatz, M. I. W.; Borresen-Dale, A. L.; Hainaut, P.; Olivier, M. TP53 mutations in human cancers: Functional selection and impact on cancer prognosis and outcomes. *Oncogene* **2007**, *26*, 2157−2165.
(17) Li, Y.; Zhang, L.; Meng, W.; Gao, Y. Dynamic changes in the urine proteome in two ovarian cancer rat models. *bioRxiv* **2019**, No. 604850.
(18) Smoot, M. E.; Ono, K.; Ruscheinski, J.; Wang, P. L.; Ideker, T. Cytoscape 2.8: New features for data integration and network visualization. *Bioinformatics* **2011**, *27*, 431−432.
(19) Győrffy, B.; Lanczky, A.; Eklund, A. C.; Denkert, C.; Budczies, J.; Li, Q.; Szallasi, Z. An online survival analysis tool to rapidly assess the effect of 22,277 genes on breast cancer prognosis using microarray data of 1,809 patients. *Breast Cancer Res. Treat.* **2010**, *123*, 725−731.
(20) Lánczky, A.; Győrffy, B.; et al. Web-based survival analysis tool tailored for medical research (KMplot): development and implementation. *J. Med. Internet Res.* **2021**, *23*, No. e27633.
(21) Liu, C.; Chen, Y.; Deng, Y.; Dong, Y.; Jiang, J.; Chen, S.; Kang, W.; Deng, J.; Sun, H. Survival-based bioinformatics analysis to identify hub genes and key pathways in non-small cell lung cancer. *Transl. Cancer Res.* **2019**, *8*, 1188−1198.
(22) Daina, A.; Michielin, O.; Zoete, V. SwissADME: a free web tool to evaluate pharmacokinetics, drug- likeness and medicinal chemistry friendliness of small molecules. *Sci. Rep.* **2017**, *7*, No. 4217.
(23) Pires, D. E. V.; Blundell, T. L.; Ascher, D. B. pkCSM: Predicting small-molecule pharmacokinetic and toxicity properties using graph-based signatures. *J. Med. Chem.* **2015**, *58*, 4066−4072.
(24) Bruker, A. X. S.*SAINT Software Reference Manual*; Bruker Analytical X-Ray Systems, Inc.: Madison, WI 5465, 1998.
(25) Sheldrick, G. M. SHELXT–Integrated space-group and crystal-structure determination. *Acta Crystallogr., Sect. A: Found. Adv.* **2015**, *71*, 3−8.
(26) López-Blanco, J. R.; Aliaga, J. I.; Quintana-Ortí, E. S.; Chacón, P. IMODS: Internal coordinates normal mode analysis server. *Nucleic Acids Res.* **2014**, *42*, 271−276.
(27) Pradhan, A.; Bepari, M.; Maity, P.; Roy, S. S.; Roy, S.; Choudhury, S. M. Gold nanoparticles from indole-3-carbinol exhibit cytotoxic, genotoxic and antineoplastic effects through the induction of apoptosis. *RSC Adv.* **2016**, *6*, 56435−56449.
(28) Dey, S. K.; Pradhan, A.; Roy, T.; Das, S.; Chattopadhyay, D.; Choudhury, S. M. Biogenic polymer-encapsulated diosgenin nanoparticles: Biodistribution, pharmacokinetics, cellular internalization, and anticancer potential in breast cancer cells and tumor xenograft. *J. Drug Delivery Sci. Technol.* **2022**, *76*, No. 103743.
(29) Kumar, S. P.; Birundha, K.; Kaveri, K.; Devi, K. T. R. Antioxidant studies of chitosan nanoparticles containing naringenin and their cytotoxicity effects in lung cancer cells. *Int. J. Biol. Macromol.* **2015**, *78*, 87−95.
(30) Niu, B.; Liao, K.; Zhou, Y.; Wen, T.; Quan, G.; Pan, X.; Wu, C. Application of glutathione depletion in cancer therapy: Enhanced ROS-based therapy, ferroptosis, and chemotherapy. *Biomaterials* **2021**, *277*, No. 121110.
(31) Gr, C.; Petrovici, S.; Olariu, L.; Trif, A. Study on the blood glutathione protective effects induced during three rats generations by $K_2Cr_2O_7$ intake. *J. Agroaliment. Processes Technol.* **2010**, *16*, 313−316.

https://doi.org/10.1021/acsomega.2c07173
ACS Omega 2022, 7, 48572−48582